

1 **Tissue-specific inhibition of protein sumoylation uncovers diverse**
2 **SUMO functions during *C. elegans* vulval development**

3

4 Aleksandra Fergin¹, Gabriel Boesch, Nadja R. Greter, Simon Berger, Alex Hajnal[°]

5

6 Institute of Molecular Life Sciences, University of Zürich, Winterthurerstrasse 190, CH-8057
7 Zürich, Switzerland

8 ¹Molecular Life Science PhD Program, University and ETH Zürich, CH-8057 Zürich,
9 Switzerland

10 [°]Corresponding author: alex.hajnal@mls.uzh.ch

11

12 **Abstract**

13 **The sumoylation (SUMO) pathway is involved in a variety of processes during *C. elegans***
14 **development, such as gonadal and vulval fate specification, cell cycle progression and**
15 **maintenance of chromosome structure. The ubiquitous expression of the sumoylation**
16 **machinery and its involvement in many essential processes has made it difficult to dissect**
17 **the tissue-specific roles of protein sumoylation and identify the specific target proteins.**
18 **To overcome these challenges, we have established tools to block protein sumoylation and**
19 **degrade sumoylated target proteins in a tissue-specific and temporally controlled**
20 **manner. We employed the auxin-inducible protein degradation system (AID) to down-**
21 **regulate AID-tagged SUMO E3 ligase GEI-17 or the SUMO ortholog SMO-1, either in**
22 **the vulval precursor cells (VPCs) or in the gonadal anchor cell (AC). Tissue-specific**
23 **inhibition of GEI-17 and SMO-1 revealed diverse roles of the SUMO pathway during**
24 **vulval development, such as AC positioning, basement membrane (BM) breaching, vulval**
25 **cell fate specification and epithelial morphogenesis. Inhibition of sumoylation in the**
26 **VPCs resulted in an abnormal shape of the vulval toroids and ectopic cell fusions.**
27 **Sumoylation of the ETS transcription factor LIN-1 at K169 mediates a subset of these**
28 **SUMO functions, especially the proper contraction of the ventral vulA toroids. Thus, the**
29 **SUMO pathway plays diverse roles throughout vulval development.**

30

31 **Introduction**

32 Sumoylation is an essential post-translational protein modification found in eukaryotes
33 (Matunis, Wu, and Blobel 1998; Mahajan et al. 1997). A major player in this pathway is the
34 so-called Small Ubiquitin-like Modifier (SUMO), which shares large structural and functional
35 similarities with Ubiquitin. However, unlike ubiquitination sumoylation promotes or inhibits
36 protein interactions and changes protein conformation or localization, allowing transient
37 binding to target proteins. Since its discovery in the late 1990s, SUMO has been shown to be
38 involved in a wide range of essential biological processes (Johnson 2004; Hay 2005; Wilkinson
39 and Henley 2010; Flotho and Melchior 2013). Though, studying its diverse functions and
40 identifying specific targets has remained challenging due to the essential roles of the SUMO
41 pathway for animal viability and development, the low concentration of sumoylated target
42 proteins, the constant activity of deSUMOylating enzymes and the often subtle effects caused
43 by the modification itself (Johnson 2004; Flotho and Melchior 2013). Developing tools, which
44 allow spatial and temporal inhibition of protein sumoylation, is therefore crucial to gain a better
45 understanding of this protein modification.

46 Protein sumoylation in *C. elegans* occurs in essentially the same fashion as in higher organisms.
47 However, contrary to mammals and other vertebrates, only one SUMO orthologue, called
48 SMO-1, exists in *C. elegans*. This renders the worm an ideal model to study this post-
49 translational protein modification system. Activated SMO-1 is transferred to the E2 enzyme
50 UBC-9 by the E1 enzyme formed by UBA-2 and AOS-1, and attached to the substrate by a
51 SUMO E3 ligase, such as the PIAS domain protein GEI-17 (Holway, Hung, and Michael 2005;
52 Ferreira et al. 2013; Pelisch et al. 2014). Deconjugation of SUMO from its targets is regulated
53 by one of four SUMO proteases, ULP-1, ULP-2, ULP-4 and ULP-5 (Pelisch et al. 2014).

54 Sumoylation is essential for *C. elegans* viability and involved in a wide range of biological
55 processes. Particularly, vulval development has previously been shown to depend on
56 sumoylation, as *smo-1(lf)* mutants exhibit multivulva (Muv) as well as protruding vulva (Pvl)
57 phenotypes (Broday 2004). We therefore chose this well-established model to further dissect
58 the different roles of the SUMO pathway during organogenesis (Schindler and Sherwood 2013;
59 Schmid and Hajnal 2015). The vulva is formed by three out of six equivalent vulval precursor
60 cells (the VPCs P3.p trough P8.p), which adopt one of three possible cell fates. The 1° fate is
61 induced in P6.p by an epidermal growth factor (EGF) signal, termed LIN-3, which is secreted
62 by the gonadal anchor cell (AC) 11/30/21 2:17:00 PM. A lateral signal from P6.p then activates
63 the LIN-12 Notch signaling pathway in the neighboring VPCs P5.p and P7.p to induce the

64 alternate, secondary (2°) fate (Greenwald, Sternberg, and Horvitz 1983; Greenwald 1985;
65 Sundaram 2004; Greenwald 2005). After vulval fate specification, the 1° VPC undergoes three
66 rounds of cell divisions producing 8 daughter cells, while the 2° fated VPCs each generate 7
67 daughter cells in an asymmetric lineage, together forming the vulva consisting of 22 cells. The
68 remaining distal VPCs (P3.p, P4.p and P8.p) adopt the uninduced 3° fate, which is to divide
69 once and fuse with the surrounding epidermis hyp7. While the VPCs proliferate, the AC
70 breaches two basement membranes (BMs) separating the uterus from the epidermis and
71 invades the underlying vulval epithelium (Sherwood and Sternberg 2003). During the
72 subsequent phase of vulval morphogenesis, the vulval cells invaginate to generate a lumen,
73 extend circumferential protrusions and fuse with their contralateral partner cells to form a
74 tubular organ consisting of a stack of seven epithelial rings called toroids (Schindler and
75 Sherwood 2013; Schmid and Hajnal 2015).

76 Here, we have employed a tissue-specific version of the auxin-inducible protein degradation
77 system (AID) to inhibit the SUMO pathway either in the AC or the vulval cells (Zhang et al.
78 2015). This approach allowed us to determine, in which tissues protein sumoylation is
79 necessary for normal vulval development, as well as to characterize the diverse phenotypes
80 caused by selectively blocking the SUMO pathway. Moreover, we hypothesized that, by
81 inserting a degron tag into SUMO itself, we could induce degradation of sumoylated proteins
82 in a tissue-specific manner. To test if this approach allows the *in vivo* identification of SUMO
83 targets, we chose LIN-1 as it was previously shown to be sumoylated at K10 and K169 by *in*
84 *vitro* experiments (Leight 2005; Leight et al. 2015). The ETS family transcription factor LIN-
85 1 is essential for different aspects of vulval development. During fate specification, LIN-1
86 inhibits VPC differentiation by recruiting transcriptional repressors in a sumoylation-
87 dependent and independent manner to repress 1° fate-specific target genes (Miley et al. 2004;
88 Leight 2005), and during morphogenesis, LIN-1 promotes the contraction of ventral toroids
89 (Farooqui et al. 2012).

90 We mutated the two known sumoylation sites in LIN-1 (K10 and K169), measured LIN-1
91 expression levels after VPC-specific degradation of AID-tagged SMO-1 and observed the
92 vulval phenotypes caused by mutation of the SUMO sites. This approach suggested that
93 sumoylation of LIN-1 in the VPCs at K169 is required for the proper contraction of the ventral
94 vulA toroid ring during morphogenesis. Additional phenotypes that were only observed after
95 degradation of GEI-17 or SMO-1 suggest that LIN-1 is one of several relevant SUMO targets
96 during vulval development.

97 This approach may be used to investigate the *in vivo* significance of potential SUMO targets
98 identified through *in vitro* experiments or by proteomic methods.

99

100 **Results**

101 **Tissue-specific, auxin-inducible degradation of SUMO pathway components**

102 To dissect the interactions of different SUMO pathway components with their substrates and
103 identify specific targets during vulval development, we adapted the tissue-specific auxin-
104 inducible degradation system (Zhang et al. 2015). Here, we generated tissue-specific
105 degradation drivers expressing the TIR-1 ubiquitin ligase in four different cell types; *hh-2p>tir-1*
106 in the AC and VU cells before and after AC specification (Sallee and Greenwald
107 2015), *cdh-3p>tir-1* in the AC post specification (Sherwood and Sternberg 2003), *egl-17p>tir-1*
108 in the 1° VPC and its descendants (Burdine, Branda, and Stern 1998) and *bar-1p>tir-1* in all
109 VPCs and their descendants (Eisenmann et al. 1998). We also used an existing driver, in which
110 TIR-1 is ubiquitously expressed under the *eft-3p>tir-1* promoter in somatic tissues (Zhang et
111 al. 2015).

112 Specificity of the degradation drivers was assessed with three assays. First, we used an SL2
113 trans-splicing acceptor to express the mCherry fluorophore under the same promoter/enhancer
114 as TIR-1. In this way tissue-specificity could be monitored by observing mCherry expression
115 (**Fig. 1A**). Second, we assessed the loss of target protein expression by degrading a GFP- and
116 AID- double tagged variant of GEI-17 (GFP::AID::GEI-17) (Pelisch et al. 2014). A strong
117 decrease in GFP::AID::GEI-17 expression upon auxin treatment was only observed in tissues
118 expressing TIR-1 (**Fig. 1B**). Lastly, we confirmed protein degradation by Western blot analysis
119 in animals expressing the pan-somatic TIR-1 driver, treated with auxin for 1h or 24h (**Fig. S1A, B**).
120 We detected only residual amounts of GEI-17 protein post degradation with comparable
121 levels for both treatment periods. The residual levels most likely stem from GEI-17 expressed
122 in the germline, where the TIR-1 driver was not expressed. Interestingly, degradation of GEI-
123 17 did not affect expression levels of SMO-1 (**Fig. S1A, C**), suggesting that depletion of GEI-
124 17 does not significantly alter the levels of free SMO-1.

125

126 **Inhibiting the SUMO pathway in the VPCs or AC causes abnormal vulval development**

127 Following the initial validation of our approach, we assessed how degradation of SUMO
128 pathway components affects vulval development. For this purpose, we crossed the different
129 TIR-1 degradation drivers with the GFP::AID::GEI-17 strain (*gei-17(fgp1)*, Pelisch et al. 2014)

130 and an N-terminally tagged AID::SMO-1 allele (*smo-1(zh140)*, this study). Note that
131 homozygous *smo-1(zh140)* animals showed a wild-type vulval morphology, but were sterile as
132 adults. Degradation of either protein using the pan-somatic TIR-1 driver resulted in
133 characteristic vulval morphogenesis defects (shown for GFP::AID::GEI-17 in **Fig. 1C**), similar
134 to chromosomal mutations in SUMO pathway genes (Broday 2004). Most adult animals
135 showed a protruding vulva (Pvl) or abnormal eversion (Evl) phenotype (Seydoux, Salvage, and
136 Greenwald 1993) of varying severity and penetrance (**Fig. 1C-E**).

137 Degrading AID::SMO-1 in all somatic cells using the *eft-3p>tir-1* driver resulted in nearly
138 completely penetrant vulval defects, while ubiquitous GEI-17 degradation caused abnormal
139 vulval development in only 65.5% (SD \pm 10.5) of the animals (**Fig. 1D, E**). Pan-somatic
140 degradation caused generally more penetrant defects than tissue-specific degradation, except
141 for depletion of AID::SMO-1 with the VPC-specific (*bar-1p>tir-1*) driver, which resulted in
142 almost fully penetrant vulval defects (97.9% SD \pm 0.6) (**Fig. 1E**). The combination of the AC
143 (*cdh-3p>tir-1*) and 1° VPC (*egl-17p>tir-1*) -specific drivers resulted in an additive effect
144 (50.2% SD \pm 5.8 combined versus 7.4% SD \pm 0.9 and 34.1% SD \pm 2.2 separate, respectively),
145 suggesting that the observed morphogenesis defects are a combination of separate functions
146 played by SMO-1 in those two tissues. By contrast, degradation of GFP::AID::GEI-17 with the
147 VPC-specific driver resulted in less penetrant defects (18.5% SD \pm 3.6), and degradation using
148 the AC and 1° VPC drivers alone or in combination did not result in significant defects (**Fig.**
149 **1D**).

150 We further investigated the defects caused by GEI-17 depletion on vulval lumen formation in
151 L4 larvae, after the toroids have been formed and the connection between vulva and uterus
152 been established (**Fig. 1F, G**). After somatic GEI-17 degradation with *eft-3p>tir-1*, 90 %
153 animals exhibited a misshaped vulval lumen, possibly due to defects in toroid fusion, cell
154 migration defects or a failure to connect the vulva to the uterus. VPC-specific degradation using
155 *bar-1p>tir-1*, on the other hand, had a less pronounced effects with only 34 % of the animals
156 showing abnormal vulval morphogenesis (**Fig. 1F, G**), suggesting that the SUMO pathway is
157 not only necessary in the VPCs but also in other tissues.

158

159 The overall lower penetrance of vulval defects observed after degrading GFP::AID::GEI-17
160 compared to AID::SMO-1 may be explained by the facts that SMO-1 is the only known SUMO
161 orthologue in *C. elegans*, whereas GEI-17 is not the only E3 ligase, and that not all sumoylation
162 reactions require an E3 ligase (Rai et al. 2011).

163

164 **The SUMO pathway acts during all stages of vulval development**

165 To determine the developmental stage, at which sumoylation is required for proper vulval
166 development, we degraded SMO-1 by exposing animals to auxin at varying developmental
167 time points between the L1/2 and L3/4 molts (**Fig. S2A**), or by withdrawing auxin at different
168 time points (**Fig. S2B**) and assessing the penetrance of the observed vulval defects.

169 In case of the *eft-3p>tir-1* and *bar-1p>tir-1* drivers, both an early auxin treatment during L1
170 until the L2 molt or a late treatment beginning in L3 caused highly penetrant vulval defects.
171 Even though there may be a slight delay until the auxin-induced effect fades after removing
172 the animals from auxin-containing medium (Zhang et al. 2015), these data point to a
173 continuous action of the SUMO pathway throughout vulval development, from VPC fate
174 specification until lumen morphogenesis.

175

176 **The SUMO pathway regulates VPC fate specification**

177 VPC fate specification occurs between the late L2 and early L3 stages and requires the
178 combined action of the Delta/Notch and EGRF/RAS/MAPK signaling pathways (Sundaram
179 2004). We first examined how inhibition of the SUMO pathway through VPC-specific
180 degradation of GEI-17 affects 1° VPC fate specification. The *egl-17* gene, which encodes an
181 FGF-like growth factor, can serve as a specific marker for the 1° VPC fate induced in response
182 to EGRF/RAS/MAPK signaling (Burdine, Branda, and Stern 1998). We thus analyzed the
183 expression of a transcriptional *egl-17>yfp* reporter after auxin-induced degradation of
184 AID::GEI-17 with the *bar-1p>tir-1* driver. *egl-17>yfp* expression was strongly reduced in the
185 1° VPC P6.p and in its descendants at the two- (Pn.px) and four-cell (Pn.pxx) stages (**Fig. 2A,**
186 **B**). The SUMO pathway therefore positively regulates 1° VPC fate specification.

187 Poulin et al. (2004) and Broday et al. (2005) previously reported that a global loss of protein
188 sumoylation in *smo-1(lf)* mutants or by *smo-1* RNAi caused the ectopic induction of additional
189 VPCs besides the three proximal VPCs (P5.p to P7.p), leading to a multivulva (Muv)
190 phenotype (Broday 2004; Poulin et al. 2005). To further quantify VPC fate specification after
191 degradation of the SUMO pathway components, we counted the numbers of induced VPCs per
192 animal after VPC-specific degradation of AID::GEI-17 (*zh142*, a *gei-17* allele containing an
193 AID but no GFP tag) or AID::SMO-1 using the *bar-1p>tir-1* driver. Vulval induction after
194 auxin-induced depletion of GEI-17 was slightly decreased (6.7% Vul, 2.96 VPCs/animal
195 induced), consistent with the reduced levels of *egl-17>yfp* (**Fig. 2A-C**). Degradation of
196 AID::SMO-1, on the other hand, resulted in a mixed phenotype with 14.3% of the animals

197 showing ectopic induction and 3.5% an underinduced phenotype, but overall only a very
198 slightly hyper-induced phenotype (3.04 VPCs/animal induced). Interestingly, we only
199 observed ectopic induction of the posterior VPC P8.p, but never of the two anterior VPCs P3.p,
200 P4.p (**Fig. 2C**).

201 Together, these data indicated that protein sumoylation in the VPCs both promotes the
202 induction of the three proximal VPCs and inhibits the differentiation of the posterior VPC P8.p.
203

204 **Sumoylation is required for proper AC positioning and symmetrical BM breaching**

205 Next, we analyzed the effects of SUMO pathway by examining AC positioning as well as BM
206 breaching. The AC in animals globally depleted of AID::GFP::GEI-17 often failed to invade
207 at the vulval midline and sometimes did not breach the BMs or breached them in an asymmetric
208 fashion (**Fig. 2D**). In addition, the AC did not fuse in 69% of the animals to form the uterine
209 seam cell syncytium (utse), which connects the vulva to the uterus, (**Fig. 2D** and **Fig. S3D**). In
210 many cases, the AC was not properly positioned at the vulval midline (quantified in **Fig. 2E** as
211 the angle of deflection from the midline), which may have led to the asymmetric or absent BM
212 breaching (quantified in **Fig. 2G**). Mispositioning of the AC and BM breaching defects were
213 only observed after somatic, but not after VPC- or AC-specific AID::GFP::GEI-17 degradation
214 (**Fig. S2A, B**), suggesting that signals from additional tissues besides the VPCs control AC
215 positioning (Ihara et al. 2011). Somatic degradation of SMO-1 also caused AC mispositioning
216 and asymmetric BM breaching (**Fig. 2E-G**). As for GEI-17, neither VPC- nor AC-specific
217 degradation of SMO-1 resulted in AC positioning or BM breaching defects (**Fig. S2A, B**)
218 In summary, our data indicate that the SUMO pathway is necessary for proper AC positioning
219 and symmetrical BM breaching during invasion. This function appears to depend on a non-
220 autonomous function of the SUMO pathway in tissues other than the AC and VPCs.
221

222 **The SUMO pathway is required for proper toroid morphogenesis**

223 Since virtually all SMO-1 and most GEI-17-depleted animals showed abnormal vulval
224 development as adults (**Fig. 1D, E**), while the VPC fate specification defects were comparably
225 rare (**Fig. 2C**), we speculated that the inhibition of protein sumoylation perturbs vulval
226 development predominantly during the later stage of morphogenesis. To characterize vulval
227 morphogenesis in more detail, we therefore examined the structure of the vulval toroids. To
228 monitor toroid formation, we used either the AJM-1::GFP or the HMR-1::GFP reporter, which
229 both label the adherens junctions between the vulval cells (Köppen et al. 2001; Marston et al.

230 2016). Degradation of SMO-1 or GEI-17 in the VPCs using the *bar-1p>tir-1* driver lead to a
231 number of different defects in toroid morphology. Specifically, we observed an abnormal shape
232 of the ventral vulA toroids (**Fig. 3A**) and ectopic fusion between the vulC and vulD or the vulA
233 and vulB1 toroids (arrows in **Fig. 3A**), similar to the defects observed in *smo-1* null mutants
234 (Broday 2004). During normal vulval morphogenesis, the ventral toroids formed by the
235 2° VPCs contract in order to extend the apical lumen dorsally (Farooqui et al. 2012). To
236 quantify ventral toroid contraction, we measured the ratio of the vulA to vulB1 diameters (**Fig.**
237 **3B**). The elevated vulA/vulB1 ratio indicated that the vulA toroids did not fully contract after
238 inhibition of the SUMO pathway in the VPCs.

239 Taken together, these data indicated that the SUMO pathway acts in the VPCs during vulval
240 toroid morphogenesis.

241

242 **Sumoylation stabilizes the LIN-1 protein in the 1° VPCs**

243 The ETS family transcription factor LIN-1 is necessary to inhibit VPC fate specification during
244 vulval induction and for the contraction of the ventral toroids during vulval morphogenesis
245 (Miley et al. 2004; Leight 2005; Farooqui et al. 2012). To assess the role of LIN-1 sumoylation
246 in vivo, we generated point mutations in the endogenous *lin-1* locus by replacing the two lysine
247 residues K10 and K169 in the SUMO consensus motifs with alanine residues (Leight 2005;
248 Leight et al. 2015). To monitor effects on LIN-1 expression levels, the two SUMO site
249 mutations were introduced into the *lin-1(st12212)* background, in which a *gfp* tag had been
250 inserted at the *lin-1* C-terminus. The wild-type *lin-1(st12212)* as well as the *lin-1(zh159)*
251 K10A, K169A double mutant reporter were then crossed with the AID::SMO-1 allele and the
252 VPC-specific *bar-1p>tir-1* driver. Wild-type LIN-1::GFP protein expression levels decreased
253 in the 1° VPC descendants, once AID::SMO-1 was degraded through addition of auxin (**Fig.**
254 **4A, B, Fig. S3A, B**). In untreated animals, LIN-1::GFP expression levels in the 2° VPC
255 descendants were lower than in the 1° cells, and LIN-1::GFP expression in the 2° cells
256 decreased only slightly after degradation of AID::SMO-1. Interestingly, the expression levels
257 of the double mutant LIN-1(K10A, K169A)::GFP protein were already lower in the 1° cells of
258 untreated animals, suggesting that sumoylation stabilizes the LIN-1 protein. Auxin-induced
259 degradation of AID::SMO-1 did not cause a further decrease in LIN-1(K10A, K169A)::GFP
260 levels in the 1° cells, indicating that the SUMO site mutations render LIN-1::GFP resistant to
261 AID::SMO-1-mediated degradation. In the 2° VPC descendants, however, a slight decrease in
262 LIN-1(K10A, K169A)::GFP levels was observed after AID::SMO-1 degradation, suggesting

263 that the sumoylation pathway may indirectly regulate LIN-1 levels in the 2° cells (**Fig. 4A, B,**
264 **Fig. S3 A, B**).

265 The reduced expression of wild-type, but not K10A, K169A double mutant LIN-1::GFP after
266 AID::SMO-1 degradation suggested that a substantial fraction of endogenous LIN-1 is
267 sumoylated in the 1° VPC descendants. These data indicated that proteasomal degradation of
268 SUMO via AID can lead to the simultaneous degradation of SUMO-modified target proteins
269 such as LIN-1. Furthermore, since LIN-1(K10A, K169A)::GFP levels were already reduced in
270 the absence of auxin when compared to wild-type LIN-1::GFP, sumoylation may stabilize the
271 LIN-1 protein. Possibly, only sumoylated LIN-1 can interact with certain binding partners to
272 form a stable complex (Leight et al. 2015). Though, we cannot exclude the possibility that the
273 K10A, K169A mutations may also affect other post-translational modifications of LIN-1, such
274 as acetylation, methylation or ubiquitination, which could also affect LIN-1 stability and
275 activity.

276

277 **The LIN-1 K169 SUMO site is necessary for ventral toroid contraction**

278 To investigate the relevance of the two SUMO sites in LIN-1, we introduced the HMR-1::GFP
279 adherens junction marker into *lin-1* single and double SUMO site mutants and investigated
280 toroid formation (*lin-1(zh157)* and *lin-1(zh158)* refer to the K10A and K169A single SUMO
281 site mutants, respectively.). In *lin-1(zh159)* K10A, K169A double and *lin-1(zh158)* K169A
282 single mutants, we observed similar toroid contraction defects as seen after AID::SMO-1 or
283 AID::GEI-17 degradation. Specifically, the ratio of the vulA to vulB1 diameter was increased
284 in *zh159* double and *zh158* single mutants (**Fig. 4C, D**). By contrast, we did not detect any
285 toroid morphogenesis defects in *lin-1(zh157)* K10A single mutants.

286 Thus, only the K169 SUMO site appears to be relevant for a specific aspect of LIN-1 function
287 during vulval toroid morphogenesis. While sumoylation of LIN-1 at K169 may be required for
288 the proper contraction of the ventral vulA toroids, none of the other defects observed after
289 inhibition of the SUMO pathway were detected in the LIN-1 SUMO site mutants. The other
290 functions of the SUMO pathway thus appear to be independent of LIN-1 sumoylation.

291

292 **Discussion**

293

294 *A tissue-specific degradation toolkit to study the SUMO pathway and its targets*

295 Posttranslational protein modification via the SUMO pathway is essential for many biological
296 processes (Deyrieux and Wilson 2017). Though, the pleiotropic effects and transient and
297 reversible nature of protein sumoylation has rendered this pathway difficult to study. The
298 identification of SUMO targets is usually performed by proteomic approaches (Matunis and
299 Rodriguez 2016; Hendriks and Vertegaal 2016) or through in vitro experiments, but the
300 possibilities to validate candidate SUMO substrates in vivo have so far been limited.

301 Here, we applied the auxin-inducible protein degradation system AID (Zhang et al. 2015) to
302 inactivate the SUMO pathway in a tissue-specific and temporally controlled manner. This
303 approach may allow the verification of relevant SUMO targets in tissues of interest by
304 following their expression levels after AID::SUMO degradation and observing the resulting
305 phenotypes.

306 Using the *C. elegans* vulva as a model for organogenesis, we dissected the role of the SUMO
307 pathway by inducing degradation of endogenously AID-tagged alleles of the SUMO homolog
308 SMO-1 and the SUMO E3 ligase GEI-17 in the different cell types contributing to the vulva.
309 For this purpose, we generated four tissue-specific TIR-1 driver lines to induce AID in the
310 tissues of interest. Tissue-specificity was validated through fluorescent co-expression markers,
311 degradation of a fluorescently tagged SUMO E3 ligase as well as protein quantification,
312 confirming the effectiveness of the toolkit. The inducible nature of the AID system allowed us
313 to assess the spatial and temporal requirements for protein sumoylation at different stages of
314 vulval development. The stronger penetrance of defects observed after degrading SMO-1 in
315 the VPCs compared to the AC suggested that sumoylation is predominantly required in the
316 VPCs. This observation is consistent with previously reported roles of SMO-1 during vulval
317 development (Miley et al. 2004; Leight et al. 2015; Ward et al. 2013). Temporally controlled
318 depletion of SMO-1 indicated that protein sumoylation is continuously required throughout
319 vulval development, controlling a variety of processes like VPC fate specification, AC
320 positioning, BM breaching and vulval toroid morphogenesis. These findings expand the range
321 of previously reported SUMO phenotypes and provide new insights in the role of sumoylation
322 during vulval development.

323 Overall, global degradation of either SMO-1 or GEI-17 resulted in stronger and more penetrant
324 phenotypes than AC- and VPC-specific degradation. This suggested that the SUMO pathway

325 acts in additional tissues besides the AC and VPCs to control vulval development. For example,
326 neurons in the ventral nerve cord are known to secrete AC guidance cues (Ziel et al. 2009),
327 while adjacent muscles can affect VPC fate specification (Moghal 2003). Degradation of SMO-
328 1 in general caused more severe phenotypes than GEI-17 degradation. This could be due to the
329 fact that SMO-1 is the only *C. elegans* SUMO homolog, while GEI-17 is one of several known
330 E3 ligases. GEI-17 may for example be replaced by MMS-21 (Rai et al. 2011), and sumoylation
331 may even occur without an E3 ligase (Gareau and Lima 2010). Moreover, proteasomal
332 degradation of AID-tagged SMO-1 appears to lead to the simultaneous degradation of
333 sumoylated target proteins, as shown here for the case of LIN-1. This may be another factor
334 explaining the stronger phenotypes observed after SMO-1 degradation compared to GEI-17
335 depletion.

336 The identification of SUMO targets is usually performed by proteomic approaches (Matunis
337 and Rodriguez 2016; Hendriks and Vertegaal 2016) or through in vitro experiments, but the
338 possibilities to validate candidate SUMO substrates in vivo have so far been limited. The
339 tissue-specific AID approach presented here may allow the verification of relevant SUMO
340 targets in specific cell types by following their expression levels after AID::SMO-1 degradation
341 and observing the resulting phenotypes.

342

343 *The SUMO pathway is required for proper BM breaching by the AC*

344 After specification of the VPC fates and before the onset of vulval morphogenesis, the AC
345 breaches two BMs separating the uterus from the vulval cells and invades at the vulval midline
346 in between the 1° vulF cells. Degradation of SMO-1 or GEI-17 resulted in characteristic AC
347 invasion defects. Occasionally, the AC completely failed to breach the underlying BMs, but a
348 more frequent defect was the displacement of the AC from the vulval midline, leading to
349 asymmetric BM breaching. Global but neither VPC- nor AC-specific degradation of GEI-17
350 or SMO-1 resulted in a displacement of the AC and asymmetrical BM breaching. However,
351 we were not able to pin-point the tissue, in which sumoylation affects AC positioning. After
352 AC invasion, the VPCs continue to proliferate and invaginate, thereby enlarging the breach in
353 the BM. The BMs then slide over the dividing vulF and vulE cells and are stabilized over then
354 un-divided vulD cells, where the INA-1/PAT-3 integrins and the VAB-19 adhesion protein are
355 expressed (Ding 2003; Ihara et al. 2011). BM sliding also depends on ventral uterine cells
356 adjacent to the AC. LIN-12 Notch signaling in the uterine π cells upregulates *ctg-1* expression,
357 which allows BM sliding by downregulating the dystroglycan BM-adhesion receptor
358 (McClatchey et al. 2016). As reported by Broday et al. (2004) and consistent with our

359 observations, sumoylation is required for the formation of a uterine lumen. The abnormal
360 connection between the vulva and uterus may in part be caused by a loss of sumoylation of
361 LIN-11 at K17 and K18 and a disruption of its function in π cells. AC positioning, on the other
362 hand, depends on guidance signals from both the VPCs and the ventral nerve cord that polarize
363 the AC along the dorso-ventral axis (Ziel et al. 2009; Naegeli et al. 2017). We thus speculate
364 that the mispositioning of the AC and asymmetrical BM breaching are caused by a cumulative
365 effect of multiple defects in different tissues.

366

367 *The SUMO pathway in the VPCs controls vulval toroid morphogenesis*

368 The most penetrant class of phenotypes caused by disruption of the SUMO pathway affects
369 vulval toroid morphogenesis. All toroid morphogenesis defects could be observed with the *bar-*
370 *Ip>tir-1* driver, indicating that these phenotypes are likely due to a cell-autonomous function
371 of the SUMO pathway in the vulval cells. Inhibiting the SUMO pathway altered *egl-17* gene
372 expression in the dividing 1° VPCs, already before the morphogenesis phase, indicating an
373 involvement of SUMO pathway during VPC induction (Leight 2005, 1; Ward et al. 2013;
374 Leight et al. 2015). Moreover, we did observe rare defects in proximal VPC induction and an
375 ectopic induction of the posterior VPC P8.p after inhibition of the SUMO pathway, which also
376 points to a role in VPC fate specification. Even though we could not directly correlate VPC
377 induction with AC positioning, it is possible that the ectopic VPC induction is at least in part
378 due to the AC mispositioning. However, the observed vulval morphogenesis defects were
379 almost fully penetrant, indicating that the SUMO pathway is most relevant during
380 morphogenesis, after the VPC fates have been specified. Protein sumoylation is required for
381 different aspects of vulval morphogenesis, such as the formation of the correct connections and
382 fusion between the contralateral pairs of vulval cells and for the contraction of the ventral vulA
383 toroids.

384

385 *LIN-1 sumoylation site at K169 promotes the contraction of the ventral vulval toroids.*

386 The ETS family transcription factor LIN-1 is a well-characterized SUMO target, originally
387 identified in genetic screens for mutants with abnormal vulval development (Miley et al. 2004;
388 Leight 2005; Leight et al. 2015). While a complete loss of *lin-1* function causes a completely
389 penetrant Muv phenotype due to loss of its repressor function, *lin-1(lf)* mutations also cause
390 reduced *egl-17* reporter expression in the 1° VPC lineage (Tiensuu et al. 2005). Moreover,
391 LIN-1 promotes ventral toroid contraction by inducing expression of the RHO kinase LET-502
392 in the 2° toroids (Farooqui et al. 2012). Together, these findings suggested that an inhibition of

393 LIN-1 sumoylation could be responsible for a subset of the similar defects caused by inhibition
394 of the SUMO pathway. Consistent with this hypothesis, expression levels of wild-type LIN-1
395 were reduced after degradation of AID::SMO-1, suggesting that LIN-1 is indeed sumoylated
396 in the vulval cells. Moreover, deletion of the K169 sumoylation site in LIN-1 caused similar
397 defects in vulA toroid contraction as VPC-specific inhibition of the SUMO pathway. We thus
398 propose that sumoylation of LIN-1 at K169 is necessary for this specific activity during vulval
399 toroid formation. Vulval fate specification, on the other hand, was not affected by deletion of
400 either of the two SUMO sites in LIN-1.

401

402 In conclusion, our findings point to complex interactions between the SUMO pathway and
403 various targets, depending on cellular context and developmental stage.

404 **Material and Methods**

405 ***C. elegans* handling and maintenance**

406 *Caenorhabditis elegans* strains were grown on standard NGM (Nematode Growth Medium)
407 plates seeded with OP50 *E. coli* bacteria and incubated at 15 °C, 20 °C or 25 °C as indicated
408 (Brenner 1974). The derivate of Bristol strain N2 was used as a wild-type reference. A list of
409 strains used in this study is provided in **suppl. Table 1**.

410

411 **Design of the tissue-specific degradation toolkit**

412 All TIR-1 degradation drivers were designed with an analogous design in the pCFJ151
413 backbone and integrated by MosSCI in selected genetic locations. To track the tissue-
414 specificity of each construct, we used an SL2 trans-splicing domain followed by an mCherry
415 reporter (fragment derived from pSA120 (Armenti et al. 2014)) to express the fluorophore
416 under the same promoter as TIR-1. In all constructs, we used the *unc-54* 3' UTR. TIR-1 was
417 amplified from pLZ31 (Zhang et al. 2015). The following promoters/enhancers were used: the
418 *egl-17* promoter was amplified as a 2042 bp fragment from a derivate of pPD107.94/mk84-
419 148 (Kirouac and Sternberg 2003), the *cdh-3* promoter was amplified as a 1897 bp fragment
420 from a derivate of pPD104.97/mk62-63 (Kirouac and Sternberg 2003; Ziel et al. 2009), the
421 *bar-1* promoter as 3216 bp fragment (Nusser-Stein et al. 2012) and the *hlh-2prox* promoter as
422 a 576 bp fragment driving the expression in two alpha and two beta cells (3VU and 1AC)
423 (Sallee and Greenwald 2015). The promoters/enhancers are indicated in text as *egl-17p*, *cdh-3p*,
424 *bar-1p* and *hlh-2p*. All constructs were cloned by Gibson assembly (Gibson et al. 2009; Gibson
425 2011). The following plasmid constructs were microinjected at the indicated final
426 concentrations into young adult EG6699, EG8078 or EG8080 hermaphrodites: transgene in
427 pCFJ150: 50 ng/μl, transformation markers pGH8 (*rap-3p>mCherry*): 10 ng/μl, pCFJ104
428 (*myop-3>mCherry*): 5 ng/μl, pCFJ90 (*myo-2p>mCherry*): 2.5 ng/μl and pJL43.1 expressing
429 Mos1 transposase: 50 ng/μl (Frøkjær-Jensen et al. 2008). The transformants were screened for
430 crawling animals, which lacked the co-injected transformation markers and genotyped for
431 homozygous insertion by PCR. The list of plasmids generated and primers used for
432 amplification of selected fragments and genotyping can be found in **suppl. Tables 2 & 3** in the
433 **Supplementary material**.

434

435 **CRISPR/Cas9 genome editing**

436 For CRISPR/Cas9 editing, the protocol by Dickinson et al. (2015) was followed. Plasmids
437 containing the repair template and single guide RNAs were used at a concentration of 10 ng/μl
438 and 50 ng/μl, respectively. We used the same transformation markers at the same
439 concentrations as for MosSCI insertions. To generate the *smo-1(zh140)* allele, an
440 oligonucleotide corresponding to a target sequence near the *smo-1* translational start site
441 (sgRNA: GCC GAT GAT GCA GCT CAA GC) was cloned into the plasmid pMW46 (derivate
442 of pDD162 from Addgene). The 5'homology arm was amplified from genomic DNA with
443 OAF239 and OAF344. The 3'homology arm was amplified with OAF345 and OAF346. The
444 AID sequence was cloned from pLZ29 with OAF334 and OAF335. The backbone of plasmid
445 containing the Self-Excising Selection Cassette was amplified in two fragments with OAF339/
446 OAF340 and OAF343/ OAF337 from pDD282.

447 To generate the *gei-17(zh142)* allele, an oligonucleotide corresponding to a target sequence
448 near the *gei-17* translational start site (sgRNA: GTC GTT TCG AGA CAC AGC GG) was
449 cloned into the plasmid pMW46. The 5'homology arm was amplified from genomic DNA with
450 OAF336 and OAF338. The 3'homology arm was amplified with OAF341/ OAF342. The
451 backbone containing the Self-Excising Selection Cassette and AID sequence was cloned in two
452 fragments with OAF334/ OAF340 and OAF343 /OAF337 from pAF56, a previously cloned
453 repair template for AID::SMO-1.

454 To generate the LIN-1 sumoylation site mutants *lin-1(zh157)* (K10A), *lin-1(158)* (K169A) and
455 *lin-1(zh159)* (K10A, K169A), genome editing was performed according to the co-CRISPR
456 strategy described by Arribere et al. (2014). To introduce the K10A mutation an
457 oligonucleotide corresponding to a target sequence (sgRNA: GTC GAG TTC GGA AGA AGC
458 CG) was cloned into plasmid pMW46. To introduce K169A mutation an oligonucleotide
459 corresponding to a target sequence (sgRNA: GTT CAT ATT TGA GGA AAA GT) was cloned
460 into the plasmid pMW46. The following constructs with indicated final concentration were
461 microinjected into young adult *lin-1(st12212)* hermaphrodites: *dpy-10* sgRNA pJA58 (25
462 ng/μl), *dpy-10* repair oligonucleotide AF-ZF-827 (0.5 nM), *lin-1* sgRNA (75 ng/μl), *lin-1*
463 repair oligonucleotide OAF377 (0.5 nM, introducing an NruI restriction site for K10A) or
464 OAF378 (0.5 nM, introducing a SacII restriction site for K169A). To generate the *zh159* double
465 mutant, the sgRNA#4 plasmid and OAF378 repair oligonucleotide was injected with the *dpy-*
466 *10* sgRNA plasmid and *dpy-10* repair oligonucleotide into *lin-1(157)* hermaphrodites at the

467 same concentrations as for the single mutant. Transformant showing a *Rol* phenotype were
468 transferred to separate NGM plates, and animals containing the desired point mutations were
469 identified by PCR amplification using the primers OAF365/ OAF366 for K10A or OAF367/
470 OAF368 for K169A, followed by restriction digests with *Nru*I or *Sac*II, respectively. The new
471 *lin-1* alleles were sequenced and back-crossed three times to N2.

472

473 **Auxin treatment**

474 NGM plates containing 1 mM auxin were prepared according to Zhang et al. (2015), seeded
475 with OP50 *E. coli* bacteria and used immediately for the experiments. The auxin treatment
476 protocol was adapted for each strain due to the differences in strain viability and fertility. For
477 strains containing AID-tagged GEI-17 (*gei-17(fgp1)* and *gei-17(zh142)* alleles), animals were
478 synchronized by bleaching, and hatched L1 larvae were plated on auxin or control plates.
479 Control plates contained the same dilution of ethanol, in which the auxin stock solution was
480 prepared, as auxin plates. Animals were incubated at 25 °C and analyzed after 24 h or 36 h of
481 treatment during the L3 or adult stage, respectively. Since homozygous *smo-1(zh140)* animals
482 are sterile, they were maintained balanced with *tmC20*, and homozygous *smo-1(zh140)* animals
483 were selected for the experiments. AID-tagged SMO-1, animals were likewise synchronized
484 by bleaching, but hatched L1 larvae were first plated on standard NGM plates containing OP50
485 and incubated at 20 °C for 24 h, followed by transfer to auxin or control plates and 24 h of
486 treatment. L3 animals were imaged right after treatment was complete, animals for analysis in
487 the adult stage were instead transferred to standard NGM plates and analyzed 24 h later. For
488 experiments involving different treatment periods, *smo-1(zh140)* animals were put on
489 auxin/control plates 12 h, 24 h, 30 h and 36 h after L1, and transferred back to standard NGM
490 plates 48 h after L1. Homozygous adults were analyzed 24 h later.

491

492 **Western blot analysis of the efficiency and kinetics of auxin-induced protein degradation**

493 40 adult animals were transferred to an Eppendorf tube containing 20 µl of water. 20 µl of
494 2xSDS buffer were added and the sample was boiled for 5 min at 95 °C. In order to digest the
495 DNA, 1 µl of DNase (Qiagen) was added, the sample was incubated for 5 min at room
496 temperature and boiled again. Proteins were separated by SDS PAGE on 4-12% acrylamide
497 gels and blotted onto PVDF membranes. After blocking non-specific binding sites with 5 %
498 milk or bovine serum albumin in TBST (20 mM Tris, 150mM NaCl, 0.1 % Tween 20), the
499 membranes were incubated with the primary antibody diluted in TBST containing 5 % milk

500 overnight at 4 °C. After incubation with HRP-conjugated secondary antibodies, the protein
501 bands were visualized by chemiluminescence using the SuperSignal West Pico or Dura
502 Chemiluminescent Substrate (Thermo Scientific). Quantification was performed by measuring
503 the band intensities using Fiji's measurement tools (Schindelin et al. 2012). The following
504 antibodies were used: anti-SUMO-1 1:500 (S5446 Sigma), anti-Flag 1:3000 (Sigma F3165-
505 1MG), anti-Tubulin 1:10 000 (Abcam ab18251), HRPGoat anti-Rabbit 1:2000 (Jackson
506 ImmunoReserach 111-035-144) and HRP Goat anti-Mouse 1:2000 (Jackson ImmunoReserach
507 115-035-146).

508

509 **Microscopy and image processing**

510 For Nomarski and fluorescence imaging, live animals were mounted on 4% agarose pads and
511 immobilized with 20 mM tetramisole hydrochloride solution in M9 buffer, unless stated
512 otherwise. For toroid analysis in *lin-1* mutants, we used a custom microfluidic devices to
513 immobilize the animals and performed imaging as described (Berger et al. 2021). Images were
514 acquired with a Leica DM6000B microscope equipped with Nomarski and fluorescence optics,
515 as well as a Leica DFC360FX camera and 63x (N.A. 1.32) oil immersion lens; a Leica DMRA
516 microscope controlled by a custom build Matlab script, equipped with an image splitter and
517 two Hamamatsu ORCA-flash 4.0L+ cameras to simultaneously acquire z-stacks in the DIC,
518 mCherry and GFP channels using a 63x (N.A. 1.32) oil immersion lens; or a Matlab controlled
519 Olympus BX61 microscope equipped with a X-light V2 spinning disc confocal system, a
520 Prizmatix UHP-T-460-DI/UHP-T-560-DI LED as light source, an Andor iXon ultra888
521 EMCCD camera and a 60x (N.A 1.3) or 100x Plan Apo (N.A 1.4) oil immersion lens. Images
522 were analyzed and quantified with Fiji software (Schindelin et al. 2012).

523

524 **Scoring vulval induction and morphogenesis**

525 The numbers of induced VPCs was scored in synchronized L4 animals as described in Schmid
526 et al. (2015). A score of 1 was assigned to a VPC when it underwent three division rounds and
527 0.5 when only one of the two VPC descendants had differentiated. A score of 0 was assigned
528 to uninduced VPCs that had divided once and fused with the hypodermis.

529 Vulval lumen morphogenesis was assessed based on DIC microscopy at the L4 stage (L4.3-
530 L4.7). Vulval defects in adult animals were scored by using a dissecting scope. Any
531 abnormality in the vulval tissue visible under a dissecting microscope was categorized as
532 'abnormal vulva' phenotype.

533

534 **Analysis of toroid formation**

535 Animals at the L4 stage were imaged either on agar pads or in microfluidic devices (Berger et
536 al. 2021) at 60x or 100x magnification, and z-stacks with a spacing of 0.13 to 0.2 μm were
537 acquired. Toroid formation was monitored using the *swIs79[ajm-1::gfp]* or *cp21[hmr-1::gfp]*
538 adherens junction markers (Diogon et al. 2007; Marston et al. 2016). Images were deconvolved
539 either by the Huygens deconvolution software (Scientific Volume imaging) or using the
540 Deconvolution lab plugin in Fiji (Schindelin et al. 2012). The measurement of the vulA and
541 vulB1 diameters was done in xz-views of the cropped ventral toroids. The toroid fusion defects
542 were scored in 3D reconstructed z-stacks.

543

544 **Quantification of LIN-1::GFP and EGL-17::YFP expression levels**

545 Animals at the mid-L3 stage were imaged at 63x magnification using a wide-field microscope,
546 acquiring z-stacks with a spacing of 0.3 μm . The average intensity of the nuclear LIN-1::GFP
547 signal was measured in background subtracted, summed z-projections of 3 mid-sagittal
548 sections of the VPCs. The nuclei of the 1° and 2° VPC descendants were manually selected,
549 and the mean nuclear signal intensity was measured using the built-in measurement tools in
550 Fiji. The data represent the averaged measurements for each VPC lineage (two nuclei at the
551 Pn.px and four at the Pn.pxx stage). *egl-17::yfp* expression levels were analyzed in background
552 subtracted mid-sagittal sections of the P6.x-P6.xxx cells. Cell bodies were manually selected,
553 and the mean intensity was measured in Fiji.

554

555 **AC mispositioning and BM breaching shift analysis**

556 Worms between L4.0-L4.5 were imaged at 63x or 100x magnification and z-stacks with a
557 spacing of 0.1-0.3 μm were acquired. The AC position was monitored based on the *qyIs50[cdh-3>mCherry::moeABD; unc-119(+)]* reporter and DIC images, and the BM breach with the
558 *qyIs10[lam-1>lam-1::gfp]* reporter. To assess the alignment of the AC with the 1° VPCs, the
559 angle between a line through the middle of the vulval invagination and the center of the ACs
560 nucleus and the dorso-ventral axis was measured, as illustrated in **Fig. 2D**. To quantify the BM
561 breaching shift, the angles α and β between the middle of the vulval invagination to each of
562 the BM breach points were measured and the ratios of the two angles was calculated (**Fig. 2D**).
563

564

565 **Statistical Analysis**

566 Statistical analysis was performed using GraphPad Prism as indicated in the figure legends.
567 Data were tested for parametric distribution and outliers were removed from analysis. For non-
568 parametric continuous data, we used the Kolmogorov-Smirnov test, for non-continuous data
569 (e.g. VPC induction counts) the Mann-Whitney test. Numerical values used for statistical
570 analysis can be found in S1_Data excel file.

571

572 **Acknowledgements**

573 We would like to thank all members of the Hajnal laboratory, Frauke Melchior, Damian
574 Brunner and Ulrike Kutay for input, and the Caenorhabditis Genetics Center (funded by NIH
575 Office of Research Infrastructure Programs (P40 OD010440)) for providing strains. This work
576 was supported by grants from the Swiss National Science Foundation no. 31003A-166580 and
577 the Swiss Cancer league no. 4377-02-2018 to AH.

578

579 **Author contributions**

580 Aleksandra Fergin: Conceptualization, Data curation, Formal analysis, Investigation,
581 Methodology, Visualization, Writing – original draft

582 Institute of Molecular Life Sciences, University of Zurich, Winterthurerstrasse, Zürich,
583 Switzerland, Molecular Life Science PhD Program, University and ETH Zurich, Zürich

584

585 Gabriel Boesch: Investigation, Methodology

586 Institute of Molecular Life Sciences, University of Zurich, Winterthurerstrasse, Zürich,
587 Switzerland, Molecular Life Science PhD Program, University and ETH Zurich, Zürich

588

589 Simon Berger: Writing – review & editing

590 Institute of Molecular Life Sciences, University of Zurich, Winterthurerstrasse, Zürich,
591 Switzerland, Molecular Life Science PhD Program, University and ETH Zurich, Zürich

592

593 Nadja Greter: Investigation

594 Institute of Molecular Life Sciences, University of Zurich, Winterthurerstrasse, Zürich,
595 Switzerland, Molecular Life Science PhD Program, University and ETH Zurich, Zürich

596

597 Alex Hajnal: Conceptualization, Investigation, Funding acquisition, Project administration,
598 Supervision, Writing – review & editing
599 Institute of Molecular Life Sciences, University of Zurich, Winterthurerstrasse, Zürich,
600 Switzerland
601

602 **References**

603 Armenti, S. T., L. L. Lohmer, D. R. Sherwood, and J. Nance. 2014. “Repurposing an
604 Endogenous Degradation System for Rapid and Targeted Depletion of *C. Elegans*
605 Proteins.” *Development* 141 (23): 4640–47. <https://doi.org/10.1242/dev.115048>.

606 Arribere, Joshua A., Ryan T. Bell, Becky X. H. Fu, Karen L. Artiles, Phil S. Hartman, and
607 Andrew Z. Fire. 2014. “Efficient Marker-Free Recovery of Custom Genetic
608 Modifications with CRISPR/Cas9 in *Caenorhabditis Elegans*.” *Genetics* 198 (3): 837–
609 46. <https://doi.org/10.1534/genetics.114.169730>.

610 Berger, Simon, Silvan Spiri, Andrew deMello, and Alex Hajnal. 2021. “Microfluidic-Based
611 Imaging of Complete *C. Elegans* Larval Development.” Preprint. Developmental
612 Biology. <https://doi.org/10.1101/2021.03.31.437890>.

613 Brenner, S. 1974. “The Genetics of *Caenorhabditis Elegans*.” *Genetics* 77 (1): 71–94.

614 Broadbent, Ian D., and Jonathan Pettitt. 2002. “The *C. Elegans* Hmr-1 Gene Can Encode a
615 Neuronal Classic Cadherin Involved in the Regulation of Axon Fasciculation.” *Current
616 Biology* 12 (1): 59–63. [https://doi.org/10.1016/S0960-9822\(01\)00624-8](https://doi.org/10.1016/S0960-9822(01)00624-8).

617 Broday, L. 2004. “The Small Ubiquitin-like Modifier (SUMO) Is Required for Gonadal and
618 Uterine-Vulval Morphogenesis in *Caenorhabditis Elegans*.” *Genes & Development* 18
619 (19): 2380–91. <https://doi.org/10.1101/gad.1227104>.

620 Burdine, R. D., C. S. Branda, and M. J. Stern. 1998. “EGL-17(FGF) Expression Coordinates
621 the Attraction of the Migrating Sex Myoblasts with Vulval Induction in *C. Elegans*.”
622 *Development (Cambridge, England)* 125 (6): 1083–93.

623 Deyrieux, Adeline F., and Van G. Wilson. 2017. “Sumoylation in Development and
624 Differentiation.” In *SUMO Regulation of Cellular Processes*, edited by Van G. Wilson,
625 963:197–214. Advances in Experimental Medicine and Biology. Cham: Springer
626 International Publishing. https://doi.org/10.1007/978-3-319-50044-7_12.

627 Ding, M. 2003. “*C. Elegans* Ankyrin Repeat Protein VAB-19 Is a Component of Epidermal
628 Attachment Structures and Is Essential for Epidermal Morphogenesis.” *Development*
629 130 (23): 5791–5801. <https://doi.org/10.1242/dev.00791>.

630 Diogon, M., F. Wissler, S. Quintin, Y. Nagamatsu, S. Sookhareea, F. Landmann, H. Hutter, N.
631 Vitale, and M. Labouesse. 2007. “The RhoGAP RGA-2 and LET-502/ROCK Achieve
632 a Balance of Actomyosin-Dependent Forces in *C. Elegans* Epidermis to Control
633 Morphogenesis.” *Development* 134 (13): 2469–79.
634 <https://doi.org/10.1242/dev.005074>.

635 Eisenmann, D. M., J. N. Maloof, J. S. Simske, C. Kenyon, and S. K. Kim. 1998. "The Beta-
636 Catenin Homolog BAR-1 and LET-60 Ras Coordinate Regulate the Hox Gene Lin-
637 39 during *Caenorhabditis Elegans* Vulval Development." *Development (Cambridge, England)* 125 (18): 3667–80.

638

639 Farooqui, Sarfarazhussain, Mark W. Pellegrino, Ivo Rimann, Matthias K. Morf, Louisa Müller,
640 Erika Fröhli, and Alex Hajnal. 2012. "Coordinated Lumen Contraction and Expansion
641 during Vulval Tube Morphogenesis in *Caenorhabditis Elegans*." *Developmental Cell*
642 23 (3): 494–506. <https://doi.org/10.1016/j.devcel.2012.06.019>.

643

644 Ferreira, Helder C., Benjamin D. Towbin, Thibaud Jegou, and Susan M. Gasser. 2013. "The
645 Shelterin Protein POT-1 Anchors *Caenorhabditis Elegans* Telomeres through SUN-1
646 at the Nuclear Periphery." *The Journal of Cell Biology* 203 (5): 727–35.
<https://doi.org/10.1083/jcb.201307181>.

647

648 Flotho, Annette, and Frauke Melchior. 2013. "Sumoylation: A Regulatory Protein
649 Modification in Health and Disease." *Annual Review of Biochemistry* 82 (1): 357–85.
<https://doi.org/10.1146/annurev-biochem-061909-093311>.

650

651 Frøkjær-Jensen, Christian, M Wayne Davis, Christopher E Hopkins, Blake J Newman, Jason
652 M Thummel, Søren-Peter Olesen, Morten Grunnet, and Erik M Jorgensen. 2008.
653 "Single-Copy Insertion of Transgenes in *Caenorhabditis Elegans*." *Nature Genetics* 40
(11): 1375–83. <https://doi.org/10.1038/ng.248>.

654

655 Gareau, Jaclyn R., and Christopher D. Lima. 2010. "The SUMO Pathway: Emerging
656 Mechanisms That Shape Specificity, Conjugation and Recognition." *Nature Reviews.
Molecular Cell Biology* 11 (12): 861–71. <https://doi.org/10.1038/nrm3011>.

657

658 Gibson, Daniel G. 2011. "Enzymatic Assembly of Overlapping DNA Fragments." In *Methods
in Enzymology*, 498:349–61. Elsevier. <https://doi.org/10.1016/B978-0-12-385120-8.00015-2>.

659

660 Gibson, Daniel G, Lei Young, Ray-Yuan Chuang, J Craig Venter, Clyde A Hutchison, and
661 Hamilton O Smith. 2009. "Enzymatic Assembly of DNA Molecules up to Several
662 Hundred Kilobases." *Nature Methods* 6 (5): 343–45.
<https://doi.org/10.1038/nmeth.1318>.

663

664 Greenwald, Iva. 1985. "Lin-12, a Nematode Homeotic Gene, Is Homologous to a Set of
665 Mammalian Proteins That Includes Epidermal Growth Factor." *Cell* 43 (3): 583–90.
[https://doi.org/10.1016/0092-8674\(85\)90230-2](https://doi.org/10.1016/0092-8674(85)90230-2).

666

667 Greenwald, Iva. 2005. "LIN-12/Notch Signaling in *C. Elegans*." *WormBook*.
668 <https://doi.org/10.1895/wormbook.1.10.1>.

669 Greenwald, Iva S., Paul W. Sternberg, and H. Robert Horvitz. 1983. “The Lin-12 Locus
670 Specifies Cell Fates in *Caenorhabditis Elegans*.” *Cell* 34 (2): 435–44.
671 [https://doi.org/10.1016/0092-8674\(83\)90377-X](https://doi.org/10.1016/0092-8674(83)90377-X).

672 Hay, Ronald T. 2005. “SUMO.” *Molecular Cell* 18 (1): 1–12.
673 <https://doi.org/10.1016/j.molcel.2005.03.012>.

674 Hendriks, Ivo A., and Alfred C. O. Vertegaal. 2016. “A Comprehensive Compilation of SUMO
675 Proteomics.” *Nature Reviews. Molecular Cell Biology* 17 (9): 581–95.
676 <https://doi.org/10.1038/nrm.2016.81>.

677 Hill, Russell J., and Paul W. Sternberg. 1992. “The Gene Lin-3 Encodes an Inductive Signal
678 for Vulval Development in *C. Elegans*.” *Nature* 358 (6386): 470–76.
679 <https://doi.org/10.1038/358470a0>.

680 Holway, Antonia H., Crystal Hung, and W. Matthew Michael. 2005. “Systematic, RNA-
681 Interference-Mediated Identification of *Mus-101* Modifier Genes in *Caenorhabditis*
682 *Elegans*.” *Genetics* 169 (3): 1451–60. <https://doi.org/10.1534/genetics.104.036137>.

683 Ihara, Shinji, Elliott J. Hagedorn, Meghan A. Morrissey, Qiuyi Chi, Fumio Motegi, James M.
684 Kramer, and David R. Sherwood. 2011. “Basement Membrane Sliding and Targeted
685 Adhesion Remodels Tissue Boundaries during Uterine–Vulval Attachment in
686 *Caenorhabditis Elegans*.” *Nature Cell Biology* 13 (6): 641–51.
687 <https://doi.org/10.1038/ncb2233>.

688 Johnson, Erica S. 2004. “Protein Modification by SUMO.” *Annual Review of Biochemistry* 73
689 (1): 355–82. <https://doi.org/10.1146/annurev.biochem.73.011303.074118>.

690 Kirouac, Martha, and Paul W. Sternberg. 2003. “Cis-Regulatory Control of Three Cell Fate-
691 Specific Genes in Vulval Organogenesis of *Caenorhabditis Elegans* and *C. Briggsae*.”
692 *Developmental Biology* 257 (1): 85–103. [https://doi.org/10.1016/s0012-1606\(03\)00032-0](https://doi.org/10.1016/s0012-1606(03)00032-0).

694 Köppen, Mathias, Jeffrey S. Simske, Paul A. Sims, Bonnie L. Firestein, David H. Hall,
695 Anthony D. Radice, Christopher Rongo, and Jeffrey D. Hardin. 2001. “Cooperative
696 Regulation of AJM-1 Controls Junctional Integrity in *Caenorhabditis Elegans*
697 Epithelia.” *Nature Cell Biology* 3 (11): 983–91. <https://doi.org/10.1038/ncb1101-983>.

698 Leight, E. R. 2005. “Sumoylation of LIN-1 Promotes Transcriptional Repression and Inhibition
699 of Vulval Cell Fates.” *Development* 132 (5): 1047–56.
700 <https://doi.org/10.1242/dev.01664>.

701 Leight, Elizabeth R., John T. Murphy, Douglas A. Fantz, Danielle Pepin, Daniel L. Schneider,
702 Thomas M. Ratliff, Duaa H. Mohammad, Michael A. Herman, and Kerry Kornfeld.

703 2015. “Conversion of the LIN-1 ETS Protein of *Caenorhabditis Elegans* from a
704 SUMOylated Transcriptional Repressor to a Phosphorylated Transcriptional
705 Activator.” *Genetics* 199 (3): 761–75. <https://doi.org/10.1534/genetics.114.172668>.

706 Mahajan, Rohit, Christian Delphin, Tinglu Guan, Larry Gerace, and Frauke Melchior. 1997.
707 “A Small Ubiquitin-Related Polypeptide Involved in Targeting RanGAP1 to Nuclear
708 Pore Complex Protein RanBP2.” *Cell* 88 (1): 97–107. [https://doi.org/10.1016/S0092-8674\(00\)81862-0](https://doi.org/10.1016/S0092-8674(00)81862-0).

710 Marston, Daniel J., Christopher D. Higgins, Kimberly A. Peters, Timothy D. Cupp, Daniel J.
711 Dickinson, Ariel M. Pani, Regan P. Moore, Amanda H. Cox, Daniel P. Kiehart, and
712 Bob Goldstein. 2016. “MRCK-1 Drives Apical Constriction in *C. Elegans* by Linking
713 Developmental Patterning to Force Generation.” *Current Biology* 26 (16): 2079–89.
714 <https://doi.org/10.1016/j.cub.2016.06.010>.

715 Matunis, Michael J., and Manuel S. Rodriguez. 2016. “Concepts and Methodologies to Study
716 Protein SUMOylation: An Overview.” *Methods in Molecular Biology* (Clifton, N.J.)
717 1475: 3–22. https://doi.org/10.1007/978-1-4939-6358-4_1.

718 Matunis, Michael J., Jian Wu, and Günter Blobel. 1998. “SUMO-1 Modification and Its Role
719 in Targeting the Ran GTPase-Activating Protein, RanGAP1, to the Nuclear Pore
720 Complex.” *Journal of Cell Biology* 140 (3): 499–509.
721 <https://doi.org/10.1083/jcb.140.3.499>.

722 McClatchey, Shelly TH, Zheng Wang, Lara M Linden, Eric L Hastie, Lin Wang, Wanqing
723 Shen, Alan Chen, Qiuyi Chi, and David R Sherwood. 2016. “Boundary Cells Restrict
724 Dystroglycan Trafficking to Control Basement Membrane Sliding during Tissue
725 Remodeling.” *eLife* 5 (September): e17218. <https://doi.org/10.7554/eLife.17218>.

726 Miley, Ginger R., Douglas Fantz, Danielle Glossip, Xiaowei Lu, R. Mako Saito, Robert E.
727 Palmer, Takao Inoue, Sander Van Den Heuvel, Paul W. Sternberg, and Kerry Kornfeld.
728 2004. “Identification of Residues of the *Caenorhabditis Elegans* LIN-1 ETS Domain
729 That Are Necessary for DNA Binding and Regulation of Vulval Cell Fates.” *Genetics*
730 167 (4): 1697–1709. <https://doi.org/10.1534/genetics.104.029017>.

731 Moghal, N. 2003. “A Component of the Transcriptional Mediator Complex Inhibits RAS-
732 Dependent Vulval Fate Specification in *C. Elegans*.” *Development* 130 (1): 57–69.
733 <https://doi.org/10.1242/dev.00189>.

734 Naegeli, Kaleb M., Eric Hastie, Aastha Garde, Zheng Wang, Daniel P. Keeley, Kacy L.
735 Gordon, Ariel M. Pani, et al. 2017. “Cell Invasion In Vivo via Rapid Exocytosis of a

736 Transient Lysosome-Derived Membrane Domain.” *Developmental Cell* 43 (4): 403-
737 417.e10. <https://doi.org/10.1016/j.devcel.2017.10.024>.

738 Nusser-Stein, Stefanie, Antje Beyer, Ivo Riman, Magdalene Adamczyk, Nir Piterman, Alex
739 Hajnal, and Jasmin Fisher. 2012. “Cell-Cycle Regulation of NOTCH Signaling during
740 *C. Elegans* Vulval Development.” *Molecular Systems Biology* 8: 618.
741 <https://doi.org/10.1038/msb.2012.51>.

742 Pelisch, Federico, Remi Sonneville, Ehsan Pourkarimi, Ana Agostinho, J. Julian Blow, Anton
743 Gartner, and Ronald T. Hay. 2014. “Dynamic SUMO Modification Regulates Mitotic
744 Chromosome Assembly and Cell Cycle Progression in *Caenorhabditis Elegans*.”
745 *Nature Communications* 5 (1): 5485. <https://doi.org/10.1038/ncomms6485>.

746 Poulin, Gino, Yan Dong, Andrew G. Fraser, Neil A. Hopper, and Julie Ahringer. 2005.
747 “Chromatin Regulation and Sumoylation in the Inhibition of Ras-Induced Vulval
748 Development in *Caenorhabditis Elegans*.” *The EMBO Journal* 24 (14): 2613-23.
749 <https://doi.org/10.1038/sj.emboj.7600726>.

750 Rai, Ragini, Satya P.M.V. Varma, Nikhil Shinde, Shilpa Ghosh, Srikala P. Kumaran, Geena
751 Skariah, and Shikha Laloraya. 2011. “Small Ubiquitin-Related Modifier Ligase
752 Activity of Mms21 Is Required for Maintenance of Chromosome Integrity during the
753 Unperturbed Mitotic Cell Division Cycle in *Saccharomyces Cerevisiae*.” *Journal of*
754 *Biological Chemistry* 286 (16): 14516-30. <https://doi.org/10.1074/jbc.M110.157149>.

755 Sallee, Maria D., and Iva Greenwald. 2015. “Dimerization-Driven Degradation of *C. Elegans*
756 and Human E Proteins.” *Genes & Development* 29 (13): 1356-61.
757 <https://doi.org/10.1101/gad.261917.115>.

758 Schindelin, Johannes, Ignacio Arganda-Carreras, Erwin Frise, Verena Kaynig, Mark Longair,
759 Tobias Pietzsch, Stephan Preibisch, et al. 2012. “Fiji: An Open-Source Platform for
760 Biological-Image Analysis.” *Nature Methods* 9 (7): 676-82.
761 <https://doi.org/10.1038/nmeth.2019>.

762 Schindler, Adam J., and David R. Sherwood. 2013. “Morphogenesis of the *Caenorhabditis*
763 *Elegans* Vulva: Morphogenesis of the *C. Elegans* Vulva.” *Wiley Interdisciplinary*
764 *Reviews: Developmental Biology* 2 (1): 75-95. <https://doi.org/10.1002/wdev.87>.

765 Schmid, Tobias, and Alex Hajnal. 2015. “Signal Transduction during *C. Elegans* Vulval
766 Development: A NeverEnding Story.” *Current Opinion in Genetics & Development* 32
767 (June): 1-9. <https://doi.org/10.1016/j.gde.2015.01.006>.

768 Schmid, Tobias, L. Basten Snoek, Erika Fröhli, M. Leontien van der Bent, Jan Kammenga, and
769 Alex Hajnal. 2015. “Systemic Regulation of RAS/MAPK Signaling by the Serotonin

770 Metabolite 5-HIAA.” Edited by Stuart K. Kim. *PLOS Genetics* 11 (5): e1005236.
771 <https://doi.org/10.1371/journal.pgen.1005236>.

772 Seydoux, Geraldine, Cathy Salvage, and Iva Greenwald. 1993. “Isolation and Characterization
773 of Mutations Causing Abnormal Eversion of the Vulva in *Caenorhabditis Elegans*.”
774 *Developmental Biology* 157 (2): 423–36. <https://doi.org/10.1006/dbio.1993.1146>.

775 Sherwood, David R, and Paul W Sternberg. 2003. “Anchor Cell Invasion into the Vulval
776 Epithelium in *C. Elegans*.” *Developmental Cell* 5 (1): 21–31.
777 [https://doi.org/10.1016/S1534-5807\(03\)00168-0](https://doi.org/10.1016/S1534-5807(03)00168-0).

778 Sternberg, P. W. 2004. “DEVELOPMENTAL BIOLOGY: A Pattern of Precision.” *Science*
779 303 (5658): 637–38. <https://doi.org/10.1126/science.1094409>.

780 Sternberg, Paul W., and H. Robert Horvitz. 1986. “Pattern Formation during Vulval
781 Development in *C. Elegans*.” *Cell* 44 (5): 761–72. [https://doi.org/10.1016/0092-8674\(86\)90842-1](https://doi.org/10.1016/0092-8674(86)90842-1).

783 Sundaram, Meera V. 2004. “Vulval Development: The Battle between Ras and Notch.”
784 *Current Biology* 14 (8): R311–13. <https://doi.org/10.1016/j.cub.2004.03.052>.

785 Tiensuu, Teresa, Morten Krog Larsen, Emma Vernersson, and Simon Tuck. 2005. “Lin-1 Has
786 Both Positive and Negative Functions in Specifying Multiple Cell Fates Induced by
787 Ras/MAP Kinase Signaling in *C. Elegans*.” *Developmental Biology* 286 (1): 338–51.
788 <https://doi.org/10.1016/j.ydbio.2005.08.007>.

789 Ward, Jordan D., Nagagireesh Bojanala, Teresita Bernal, Kaveh Ashrafi, Masako Asahina, and
790 Keith R. Yamamoto. 2013. “Sumoylated NHR-25/NR5A Regulates Cell Fate during *C.*
791 *Elegans* Vulval Development.” Edited by David J. Mangelsdorf. *PLoS Genetics* 9 (12):
792 e1003992. <https://doi.org/10.1371/journal.pgen.1003992>.

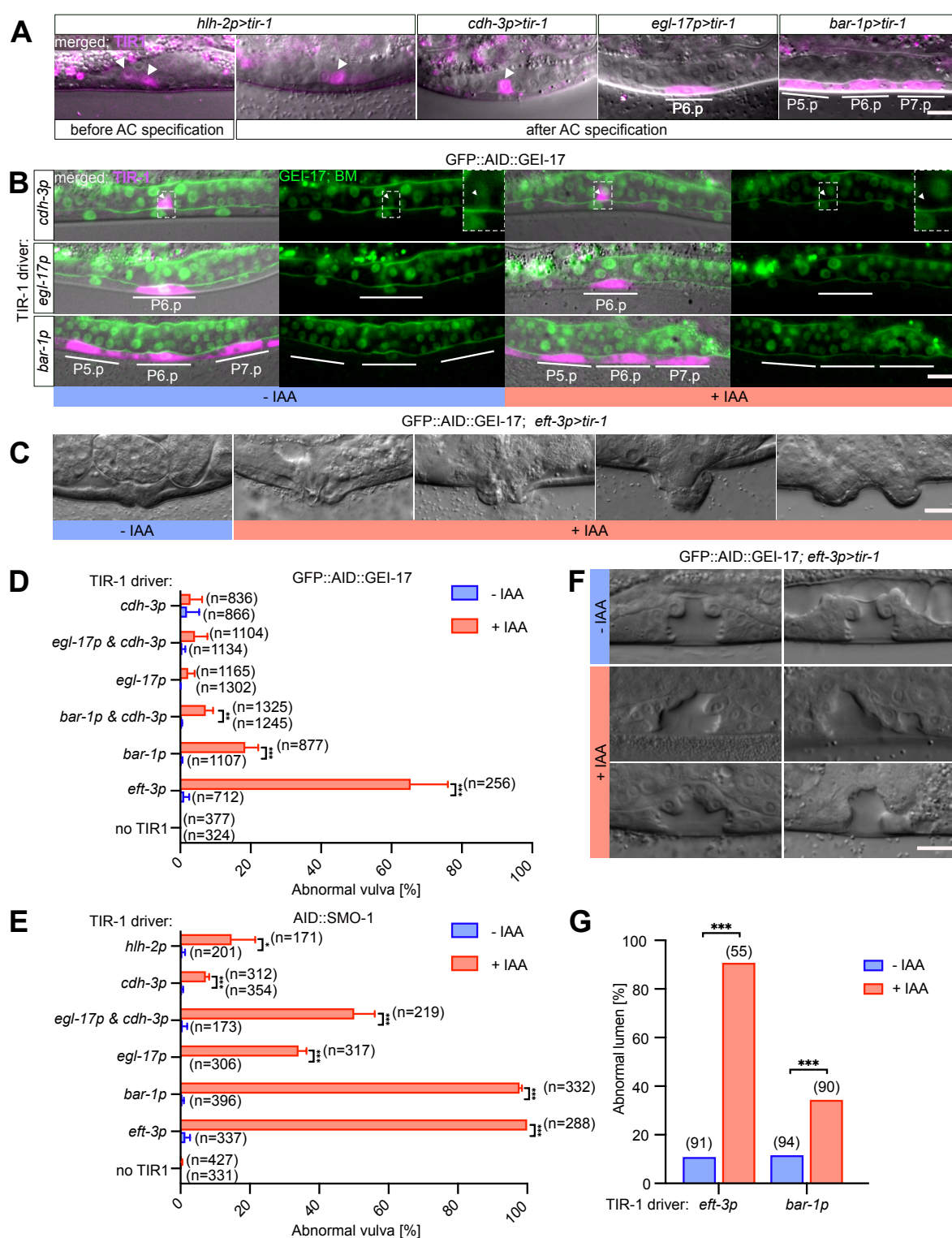
793 Wilkinson, Kevin A., and Jeremy M. Henley. 2010. “Mechanisms, Regulation and
794 Consequences of Protein SUMOylation.” *Biochemical Journal* 428 (2): 133–45.
795 <https://doi.org/10.1042/BJ20100158>.

796 Zhang, L., J. D. Ward, Z. Cheng, and A. F. Dernburg. 2015. “The Auxin-Inducible Degradation
797 (AID) System Enables Versatile Conditional Protein Depletion in *C. Elegans*.”
798 *Development* 142 (24): 4374–84. <https://doi.org/10.1242/dev.129635>.

799 Ziel, Joshua W., Elliott J. Hagedorn, Anjon Audhya, and David R. Sherwood. 2009. “UNC-6
800 (Netrin) Orients the Invasive Membrane of the Anchor Cell in *C. Elegans*.” *Nature Cell
801 Biology* 11 (2): 183–89. <https://doi.org/10.1038/ncb1825>.

802

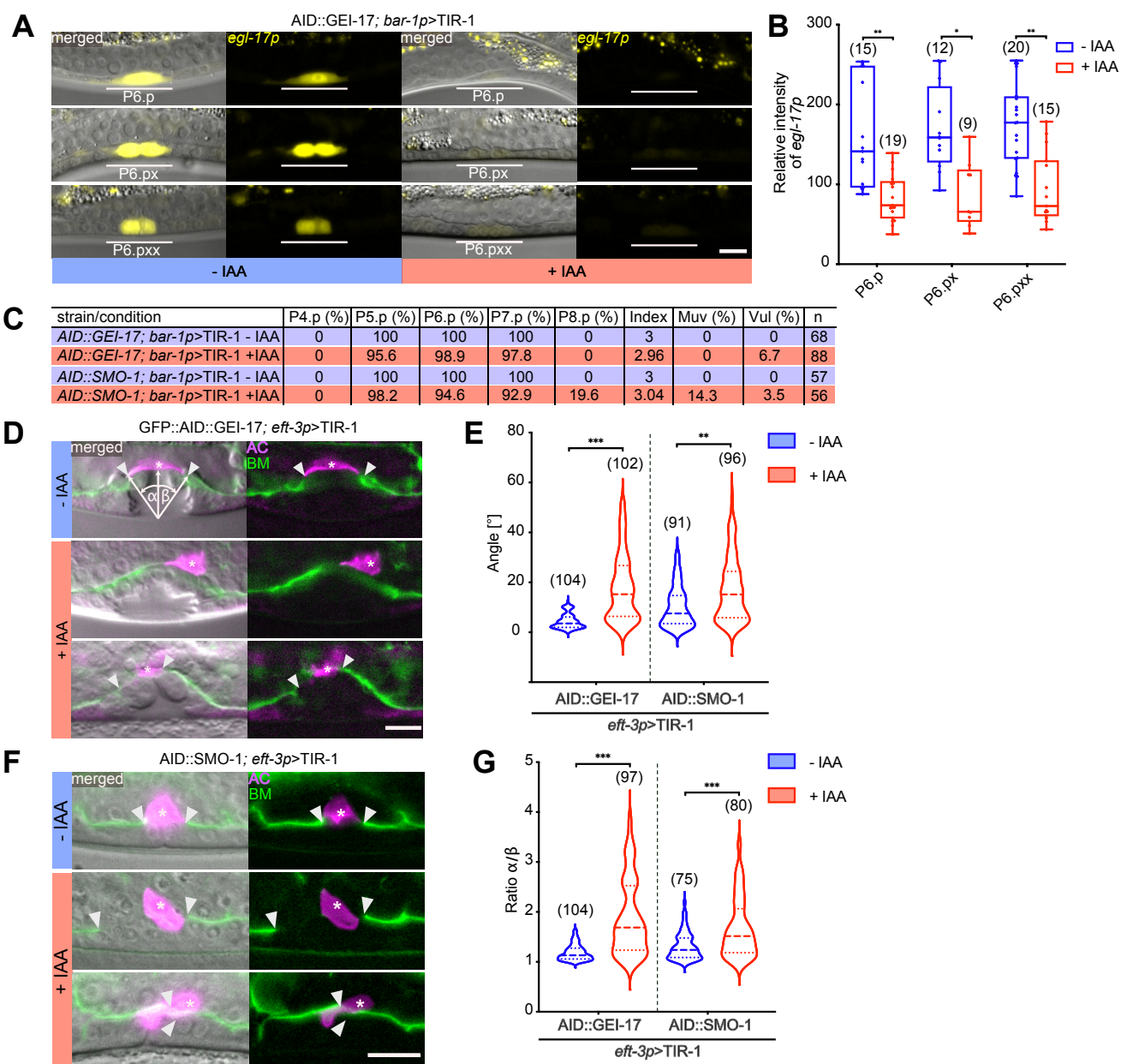
803 **Figures**



804

805

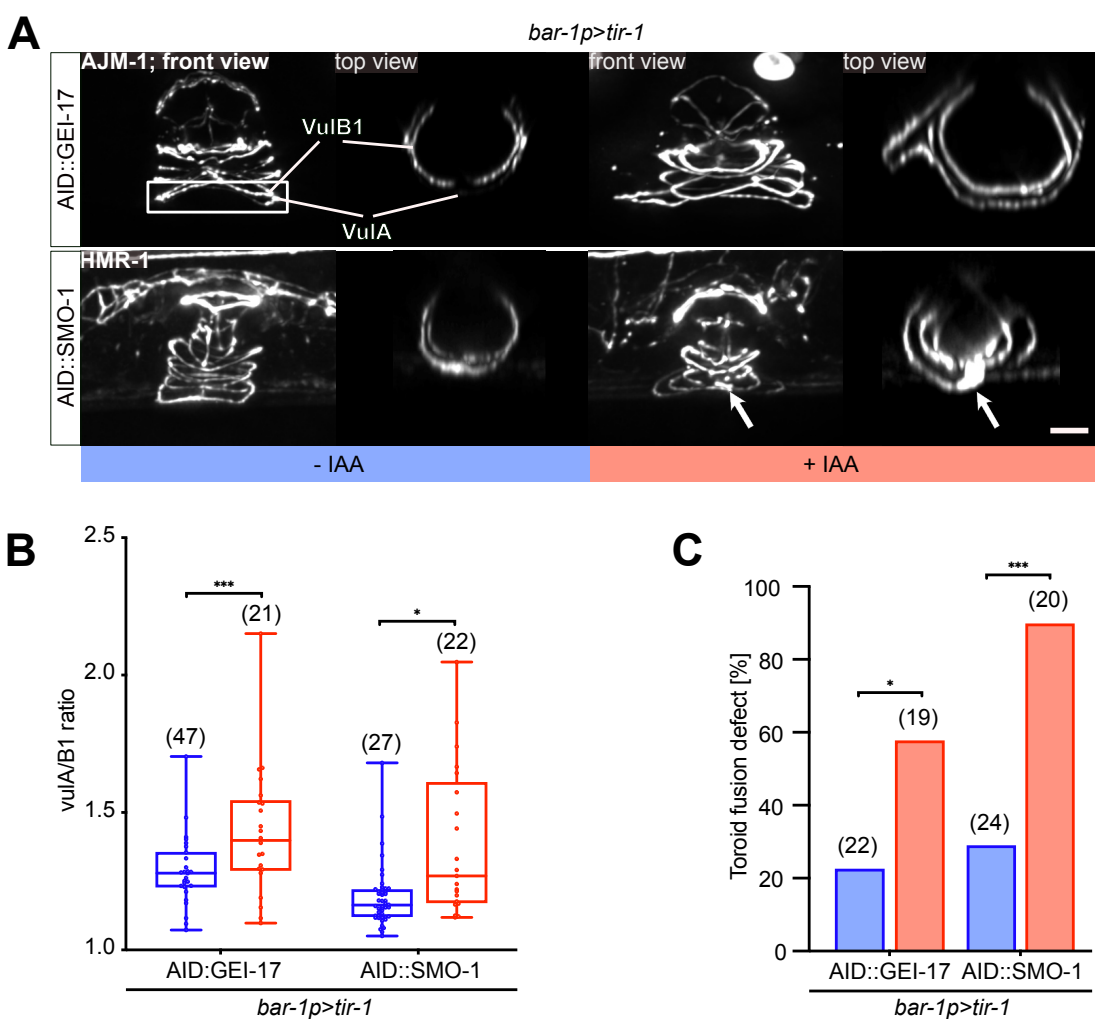
806 **Fig 1. Degradation of SUMO pathway components leads to abnormal vulval development**
807 **(A)** Tissue-specific expression of the TIR-1::SL2::mCherry degradation driver using the
808 indicated TIR-1 drivers. mCherry expression from the bi-cistronic mRNA in magenta overlaid
809 with the corresponding DIC images is shown for each transgene. White arrowheads indicate
810 the AC and bars outline the location of the VPCs. **(B)** Tissue-specific degradation of
811 GFP::AID::GEI-17 after auxin treatment using the indicated TIR-1 drivers. Left panels show
812 the TIR-1::SL2::mCherry expression in magenta overlaid with the GFP::AID::GEI-17 and
813 LAM-1::GFP BM markers in green and the corresponding DIC images. Right panels show
814 only the GFP::AID::GEI-17 signal along with the LAM-1::GFP marker in green. White lines
815 outline the location of the VPCs. The insets in the top row show the region around the AC
816 magnified around 3x, indicated by white arrowhead. **(C)** DIC images illustrating the vulval
817 morphology defects in adults after global degradation of GFP::AID::GEI-17. **(D)** Penetrance
818 of the vulval morphology defects after auxin-induced degradation of GFP::AID::GEI-17 and
819 **(E)** AID::SMO-1 using the indicated TIR-1 drivers. The mean values \pm s.d. obtained from three
820 biological replicates are shown. **(F)** DIC images of L4 larvae showing an abnormally shaped
821 vulval lumen resulting after global GFP::AID::GEI-17 degradation. **(G)** Penetrance of the
822 vulval morphogenesis defects shown in **(F)** using the global *eft-3p* and VPC-specific *bar-*
823 *Ip>tir-1* drivers. Treatment conditions are indicated as +IAA (blue) for animals treated with 1
824 mM auxin, and -IAA (red) for control animals. All GFP::AID::GEI-17 animals were treated at
825 25 °C from the L1 stage onward. All AID::SMO-1 were treated at 20 °C from the L2 to L4
826 stage. In **(D)** and **(E)** the numbers of animals scored are indicated in brackets. Statistical
827 significance was determined by two-tailed unpaired t-tests **(D, E)** or with Mann-Whitney tests
828 **(G)**. Asterisks indicate the p-values as * $p \leq 0.05$; ** $p \leq 0.01$; *** $p \leq 0.001$. The scale bars are
829 10 μm.
830



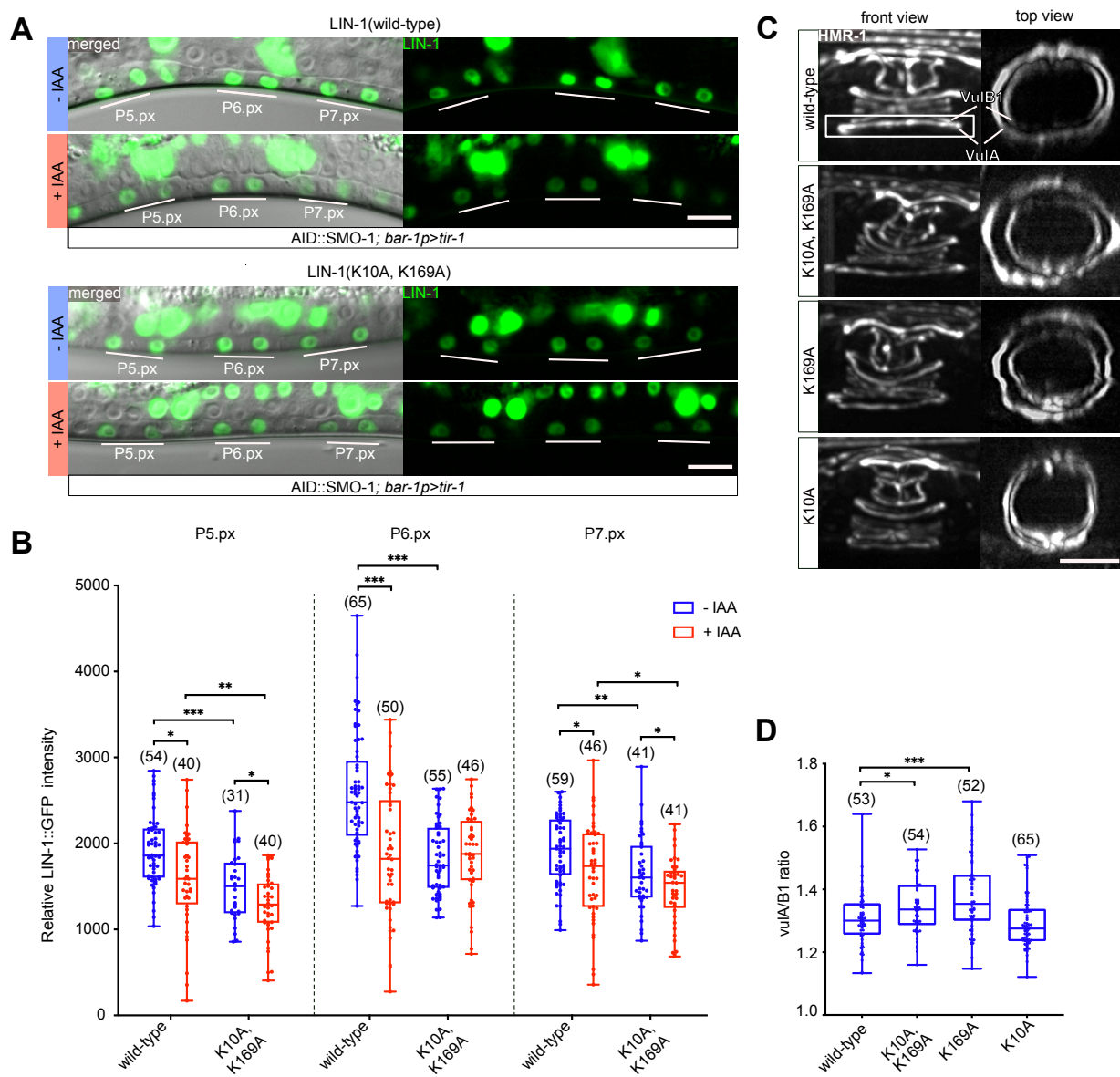
832 **Fig 2. The SUMO pathway regulates vulval development**

833 **(A)** *egl-17p>yfp* expression in P6.p and its descendants P6.px and P6.pxx after VPC-specific
834 degradation of GEI-17. **(B)** Quantification of *egl-17p>yfp* expression levels after AID::GEI-
835 17 depletion. Box plots show the median values with the 25th and 75th percentiles and whiskers
836 indicate the maximum and minimum values. **(C)** VPC induction upon degradation of
837 AID::GEI-17 and AID::SMO-1. For each strain and condition, the percent of induced VPCs,
838 the average number of induced VPCs per animal (index), percent of multivulva (Muv, index>3)
839 and vulvaless (Vul, index <3) animals, and the number of animals scored (n) are shown. **(D)**
840 AC displacement, AC fusion defects and asymmetric BM breaching after global AID::GEI-17
841 and **(F)** AID::SMO-1 degradation. The BMs are labelled with LAM-1::GFP in green and the
842 AC with *cdh-3p>mCherry::moeABD* in magenta. White arrowheads indicate the borders of
843 the BM breaches and asterisks the AC. The left panels show the fluorescent signals merged
844 with the corresponding DIC images. The angles α and β used to quantify AC alignment and
845 symmetry of the BM breaching are illustrated in the top left panel. **(E)** Quantification of the
846 AC displacement and **(G)** BM breaching asymmetry after degradation of GEI-17 and SMO-1
847 using the global *eft-3p>tir-1* driver. See also **suppl. Fig. S3** for the results obtained with tissue-
848 specific *tir-1* drivers. Dashed lines in the violin plots **(E, G)** show the median values and the
849 dotted lines the 25th and 75th percentiles. In all experiments, untreated controls are labelled with
850 –IAA (blue) and animals treated with 1 mM auxin +IAA (red). In each graph, the numbers of
851 animals scored are indicated in brackets. Statistical significance was determined with a
852 Kolmogorov-Smirnov test **(B, E, G)**. p-values are indicated as * p≤0.05; ** p≤ 0.01; *** p≤
853 0.001. The scale bars are 10 μ m.

854



857 **Fig. 3. Inhibition of the SUMO pathway in the VPCs causes toroid morphogenesis defects**
858 **(A)** Toroid morphogenesis defects in L4 hermaphrodites. 3D reconstructions of the adherens
859 junctions labelled with AJM-1::GFP (for AID::GEI-17) or HMR-1::GFP (for AID::SMO-1)
860 after VPC-specific degradation. Left panels show lateral views of z-projections. vulA and
861 vulB1 toroids are outlined by the white rectangle in the top left panel and shown in top (xz)
862 views in the right panels. White arrows point to abnormal fusion between the vulA and vulB1
863 toroids after AID::SMO-1 degradation. **(B)** Quantification of vulA contraction, calculated as
864 the ratio of the vulA and vulB1 toroid diameter after VPC-specific AID::GEI-17 or AID::SMO-
865 1 degradation. The box plots show the median values with the 25th and 75th percentiles and the
866 whiskers indicate the maximum and minimum values. **(C)** Penetrance of toroid fusion defects
867 after VPC-specific AID::GEI-17 or AID::SMO-1 degradation. In all experiments, untreated
868 controls are labelled with -IAA (blue) and animals treated with 1 mM auxin +IAA (red). In
869 each graph, the numbers of animals scored are indicated by the numbers in brackets. In **(B)**
870 unpaired two-tailed t-tests and in **(C)** Mann-Whitney tests were used to determine statistical
871 significance. p-values are indicated as * p≤0.05; ** p≤ 0.01; *** p≤ 0.001. The scale bar is
872 10 μm.



873

874

875 **Fig. 4. LIN-1 sumoylation is required for ventral toroid contraction**

876 **(A)** Wild-type and K10A, K169A mutant LIN-1::GFP expression in L3 larvae at the Pn.px
877 stage after VPC-specific degradation of AID::SMO-1 from the L2 stage onward. The 1° and
878 2° VPC descendants are underlined in white. The left panels show the corresponding DIC
879 images overlaid with the LIN-1::GFP signal in green. **(B)** Quantification of LIN-1::GFP
880 expression levels in 1° and 2° VPC descendants at the Pn.px stage in LIN-1::GFP wild-type
881 and K10A, K169A double mutants under the indicated conditions. See **suppl. Fig. S4** for the
882 corresponding measurements at the Pn.pxx stage. **(C)** Toroid morphogenesis defects in LIN-1
883 K10A and K169A single and double mutants at the L4 stage. Left panels show lateral views of
884 z-projections. vulA and vulB1 toroids are outlined by the white rectangle in the top left panel
885 and shown in top (xz) views in the right panels. **(D)** Quantification of vulA contraction,
886 calculated as the ratio of the vulA and vulB1 toroid diameter. The box plots show the median
887 values with the 25th and 75th percentiles and the whiskers indicate the maximum and minimum
888 values. Where indicated, untreated controls are labelled with -IAA (blue) and animals treated
889 with 1 mM auxin with +IAA (red). In each graph, the numbers of animals scored are indicated
890 by the numbers in brackets. Statistical significance in **(B)** and **(D)** was calculated with unpaired
891 two-tailed t-tests. p-values are indicated as * $p \leq 0.05$; ** $p \leq 0.01$; *** $p \leq 0.001$. The scale bars
892 are 10 μ m.